

# The Excess Density of Field Galaxies near $z \sim 0.56$ around the Gamma-Ray Burst GRB 021004 Position

I. V. Sokolov,<sup>1,\*</sup> A. J. Castro-Tirado,<sup>2</sup> O. P. Zhelenkova,<sup>3,4</sup>

I. A. Solovyev,<sup>5</sup> O. V. Verkhodanov,<sup>3</sup> and V. V. Sokolov<sup>3</sup>

<sup>1</sup>*Institute of Astronomy, Russian Academy of Sciences, Moscow, 119017 Russia*

<sup>2</sup>*Stellar Physics Department, Institute for Astrophysics of Andalusia (IAA-CSIC), Granada, 18008 Spain*

<sup>3</sup>*Special Astrophysical Observatory, Russian Academy of Sciences, Nizhnii Arkhyz, 369167 Russia*

<sup>4</sup>*ITMO University, St. Petersburg, 197101 Russia*

<sup>5</sup>*Astronomical Department, St. Petersburg State University, St. Petersburg, 199034 Russia*

We test for reliability any signatures of field galaxies clustering in the GRB 021004 line of sight. The first signature is the GRB 021004 field photometric redshifts distribution based on the 6-m telescope of the Special Astrophysical Observatory of the Russian Academy of Sciences observations with a peak near  $z \sim 0.56$  estimated from multicolor photometry in the GRB direction. The second signature is the Mg II  $\lambda\lambda 2796, 2803 \text{ \AA}$  absorption doublet at  $z \approx 0.56$  in VLT/UVES spectra obtained for the GRB 021004 afterglow. The third signature is the galaxy clustering in a larger (of about  $3^\circ \times 3^\circ$ ) area around GRB 021004 with an effective peak near  $z \sim 0.56$  for both the spectral and photometric redshifts from a few catalogs of clusters based on the Sloan Digital Sky Survey (SDSS) and Baryon Oscillation Spectroscopic Survey (BOSS) as a part of SDSS-III. From catalog data the size of the whole inhomogeneity in distribution of the galaxy clusters with the peak near  $z \approx 0.56$  is also estimated as about  $6^\circ\text{--}8^\circ$  or 140–190 Mpc. A possibility of inhomogeneity (a galaxy cluster) near the GRB 021004 direction can be also confirmed by an inhomogeneity in the cosmic microwave background related with the Sunyaev–Zeldovich effect.

## 1. INTRODUCTION

The main motivation in conducting this work is a number of additional new studies on the Great Walls in increasing order of redshift  $z$ :

- Paper [1] deals with the Sloan Great Wall superclusters in the redshift range  $0.04 < z < 0.12$ . The authors explore how unusual are the Shapley Supercluster (with  $z = 0.046$ ) and the Sloan Great Wall, considering the Sloan Great Wall as a complex of superclusters with collapsing

---

\* Electronic address: sok334455@mail.ru

cores [2]. In these papers the distribution of galaxy groups in the Sloan Great Wall superclusters in the sky plane is studied in detail.

- The BOSS Great Wall superclusters in the redshift range  $0.43 < z < 0.71$  were studied in paper [3], it deals with discovery of a massive supercluster system at  $z \sim 0.47$ . The BOSS Great Wall consists of two walls with diameters about 186 and 173 Mpc, and two other major superclusters with diameters of about 64 and 91 Mpc. This system consists of 830 galaxies with the mean  $z = 0.47$  and with the total mass approximately  $2 \times 10^{17} M_{\odot}$ . The authors emphasize that the morphology of the superclusters in the BOSS Great Wall system is similar to the morphology of the superclusters in the Sloan Great Wall.
- Paper [4] concerns some new Large Quasar Group (Huge-LQG) at  $z \sim 1.3$ . It was the study of sky distribution of 73 quasars ( $z = 1.27$ ) of the new Huge-LQG, together with that of 34 quasars of the Clowes-Cappusano Large Quasar Group (CCLQG) with  $z = 1.28$  [5]. “Huge-LQG” is the area of about  $29^{\circ}5 \times 24^{\circ}0$ . The members of each LQG are connected at the linkage scale of 100 Mpc.
- Here it should be said also about a giant ring-like structure at  $0.78 < z < 0.86$  displayed by GRBs themselves, which is discussed in paper [6]. This appears to indicate the presence of some real density enhancement at about 2800 Mpc. The possible structure in the GRB sky distribution is also discussed in [7]. This huge GRB structure lies ten times farther away than the Sloan Great Wall, at a distance of approximately ten billion light years. The size of the structure defined by these GRBs is about 2000–3000 Mpc, or six times larger than the size of the Sloan Great Wall.
- Paper [8] deals with statistics of the Planck CMB signal in direction of GRBs from the BATSE and *BeppoSAX* catalogs or on a possible inhomogeneity (non-Gaussianity) in the GRB sky distribution. So, although the apparent distribution of GRBs in the sky was proven to be isotropic [9] some studies have pointed out to a possible correlation with a nonuniformity of the cosmic microwave background (CMB) [8] and clustering of GRBs at intermediate redshifts has been also reported [6]. Besides this, a possible clustering of neutrino signals in relation with GRBs has been also discussed [10].

The Mg II  $\lambda\lambda 2796, 2798\text{\AA}$  absorption doublet in the joint redshift range of the above-mentioned Huge-LQG (Large Quasar Group at  $z \sim 1.3$ ) has been found in spectra of background quasars (with  $z \gtrsim 1.4$ ), using the Mg II absorber catalogue of Raghunathan et al. of 2016 [11]. Another work [12] presents statistics from a survey for intervening Mg II absorption towards 100 quasars with emission (proper) redshifts between  $z = 3.55$  and  $z = 7.08$ . So, the quasar spectroscopy relies

on using some strong detecting galaxy clusters. So, GRB afterglow spectroscopy also can reveal intervening systems along the line of sight. The clustering of galaxies and the clustering around GRB sight-lines are detected and studied in the same manner employed with quasar spectroscopy in many papers already (see [13] and references therein) because GRBs originate at cosmological distances with energy releases of  $10^{51}$ – $10^{53}$  erg at a range of redshifts between about 0.01 and more than 9.2. And long-duration GRBs are beacons of starforming galaxies (see references in [14]) up to very high redshifts.

Galaxies that give rise to the absorption line systems in GRBs afterglow spectra have been directly imaged and investigated. So, it is possible to try to find the overdensity excess of GRB field galaxies around GRB positions by different methods: spectroscopic, photometric ones (using deep images and multiband photometry) plus the search for a correlation with Cosmic Microwave Background (CMB). The data from new redshift catalogs of galaxy clusters can be used also to estimate size of these galaxy superclusters in regions near the GRB positions. In particular, in this paper we test for reliability any signatures of field galaxies clustering in GRB 021004 line of sight and in the larger areas around the GRB.

## 2. ON THE OBSERVATIONAL DATA AND METHODOLOGY OF THEIR INTERPRETATION

Here the 6-m telescope of the Special Astrophysical Observatory (BTA) observational data are the base of our investigations. The deep fields reported in Table 1 were studied with BTA (before 2002) under the program of GRBs monitoring, starting from the very first optical identifications of their GRB afterglows. Hereby, all these BTA observations were carried out in the course of the search and study of GRB host galaxies and comparison of their properties with those of all observable galaxies in GRB deep fields. Papers [15, 16] describe the methodology of processing and interpretation of these observations, which can be used now in new tasks on the study of distribution of galaxy clusters in GRB directions [13, 17–19]. In particular, to study the GRB 021004 field we used the methodology already developed for the *BVRI* deep field of GRB 000926 (see Table 1), which was investigated with BTA and the results were published [15]. This work presents the observations of a  $3'6 \times 3'$  field centered on the GRB 000926 host galaxy position at coordinates  $RA(J2000) = 17^h04^m11^s$ ,  $Dec(J2000) = +51^\circ4'9''.8$ . Hereafter notations RAJ and DecJ are used. The observations were carried out on the BTA using the SCORPIO instrument [20]. The catalog of galaxies detected in this GRB 000926 field includes 264 objects, for which the signal-to-noise ratio is

**Table 1.** Deep fields around gamma-ray bursts observed with BTA in 1987–2002

GRB	Bands	Exposure time, s
970508	<i>BVRI</i>	$600 \times 7, 500 \times 4, 600 \times 5, 400 \times 5$
971214	<i>VR</i>	$600 \times 1, 600 \times 1$
980613	<i>BVRI</i>	$700 \times 1, 600 \times 1, 600 \times 3$
980703	<i>BVRI</i>	$480 \times 1, 320 \times 1, 300 \times 1, 360 \times 1$
990123	<i>BVRI</i>	$600 \times 1, 600 \times 1, 600 \times 1, 600 \times 1$
991208	<i>BVRI</i>	$300 \times 6, 300 \times 5, 180 \times 7, 180 \times 2$
000926	<i>BVRI</i>	$500 \times 5, 300 \times 5, 180 \times 25, 120 \times 15$
021004	<i>BVRI</i>	$600 \times 6, 450 \times 13, 180 \times 15, 120 \times 14$

larger than 5 in each photometric band. The following limiting magnitudes were derived:  $26^m6$  (*B*),  $25^m0$  (*V*),  $25^m8$  (*R<sub>c</sub>*), and  $24^m5$  (*I<sub>c</sub>*). The differential galaxy counts are in good agreement with previously published CCD observations of the deep fields. The photometric redshifts for all of the cataloged objects and the corresponding color variations of the galaxies as a function of the redshift were derived. As a result, for luminous spiral galaxies with  $M_B < 18$ , no evidence for any noticeable evolution of their linear sizes to  $z \sim 1$  was found.

For studying other deep fields listed in Table 1 these data were supplemented with other data obtained with other instruments for GRB 021004, GRB 970508, and others, including investigation of the surroundings of the radio source RC J0311+0507 [21].

And as was mentioned above, the GRB 021004 field was studied as a part of GRB afterglow observations program [15, 16]. Exposure times for this field were of about one hour in each of the *BVRI* optical bands (see Table 1). We used the SExtractor software package [22] to extract objects from the stacked *BVRI* image. The catalog of galaxies, extracted from this field of size  $4' \times 4'$  includes 935 objects for which magnitude errors are not larger than  $0^m1$  (see Fig. 1, left). So, the following limiting magnitudes were achieved for these BTA observations of the GRB 021004 field:  $26^m9$  (*B*),  $27^m2$  (*V*),  $26^m0$  (*R<sub>c</sub>*) and  $25^m5$  (*I*).

One of the goals of this work is to point out the possibility of using the 6-m telescope in these challenging and actual tasks to supplement mentioned studies with other instruments' data. We also made sure our results of deep photometry are consistent with the corresponding HST ACS data<sup>1</sup> for the GRB 021004 field. Figure 1 (right) represents data acquired with HSC ACS camera in *F475W*, *F606W* and *F814W* optical bands with the magnitude errors no larger than 0.1 for

<sup>1</sup> Hubble Legacy Archive, <http://hla.stsci.edu/hlaview.html>

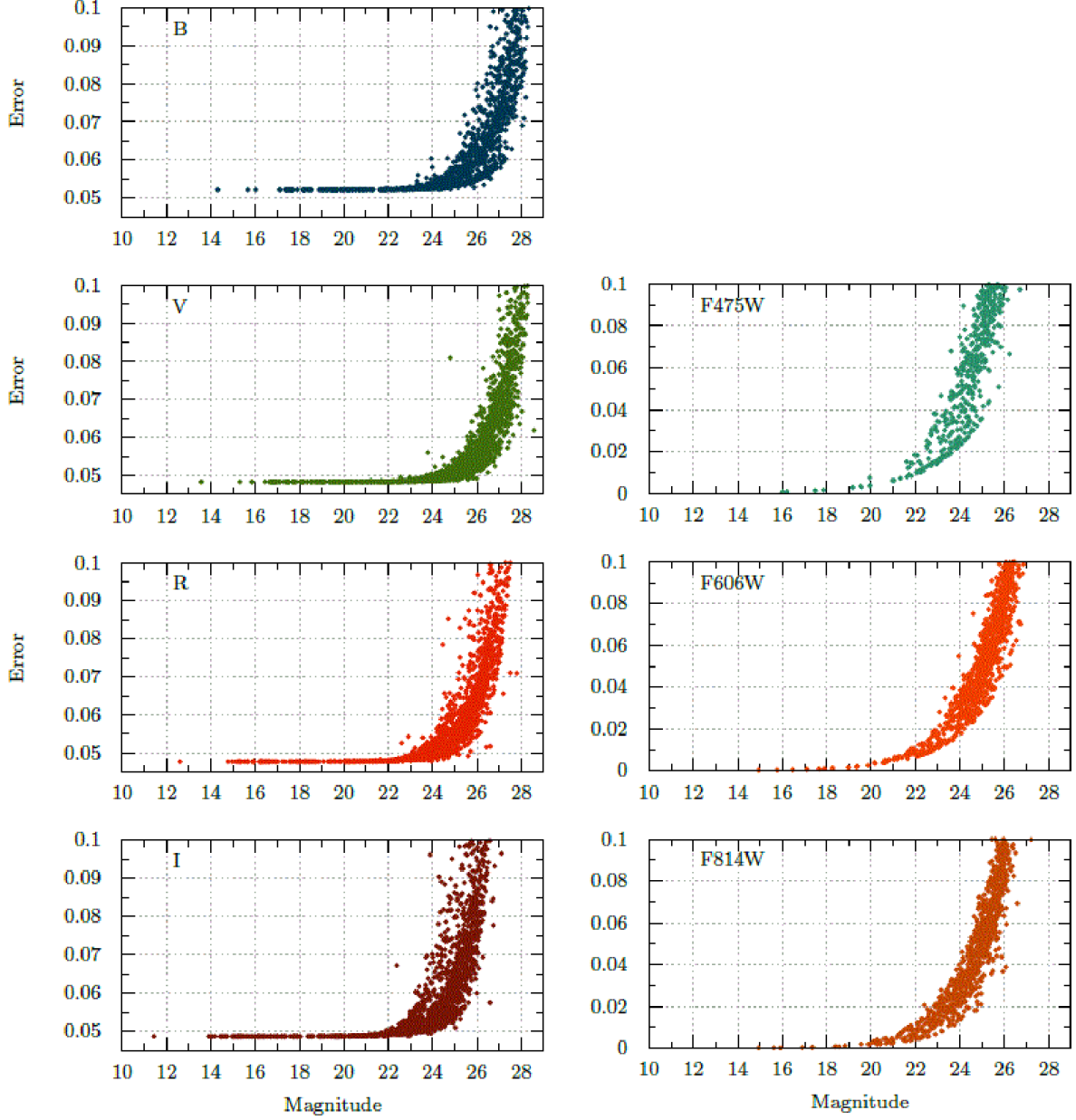


**Figure 1.** The magnitude-error diagram for objects extracted from the GRB021004 field. Left column graphs represent data of BTA *BVRI* bands. Right column graphs represent data for the same field acquired with HST ACS camera in *F475W*, *F606W* and *F814W* optical bands (Hubble Legacy Archive, <http://hla.stsci.edu/hlaview.html>).

the same extended objects, whose *BVRI* photometry was made with BTA. Figure 2 shows the filter transmission curves of BTA *BVRI* optical bands and also HST ACS optical bands *F475W*, *F606W*, *F814W* for comparison. Here we did not use directly these HST ACS data (Fig. 1, right) for the photometric redshift estimations, since the filter transmission curves of BTA *BVRI* and the HST ACS optical bands overlap. But the main thing is that the same HST ACS data can be used

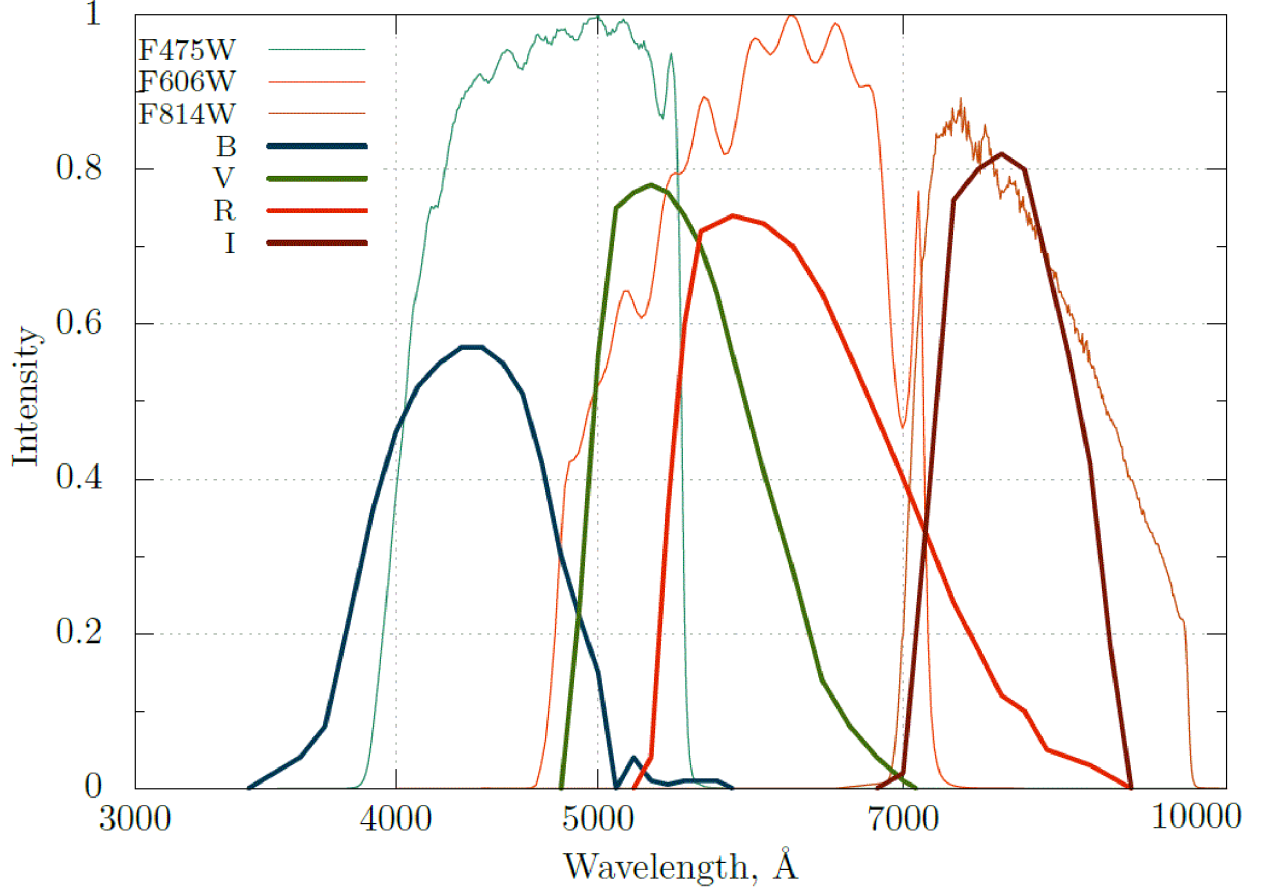


**Figure 2.** Filter transmission curves of BTA *BVRI* and HST ACS (*F475W*, *F606*, *F814W*) optical bands.

**Table 2.** The estimates of photometric  $z$ , with the probability of the photo- $z$  measurements for the seven galaxies with known morphology near the GRB 021004 position (see Fig. 3 and the text)

Num	$R$ , mag	$z$	%	Type
227	20.60	0.435	82	S0
311	21.82	0.40	94	Burst
121	21.16	0.42	84	Sa
123	21.41	0.40	98	E
147	21.61	0.44	86	E
314	21.58	0.46	95	Burst
295	20.60	0.41	92	S0

also for obtaining information on morphology of HST/BTA objects (see Fig. 3).

The HST photometry of extended objects in the GRB 021004 field is adduced here for comparison with data of BTA *BVRI* photometry of the same objects. In particular, as is seen in Fig. 1, the

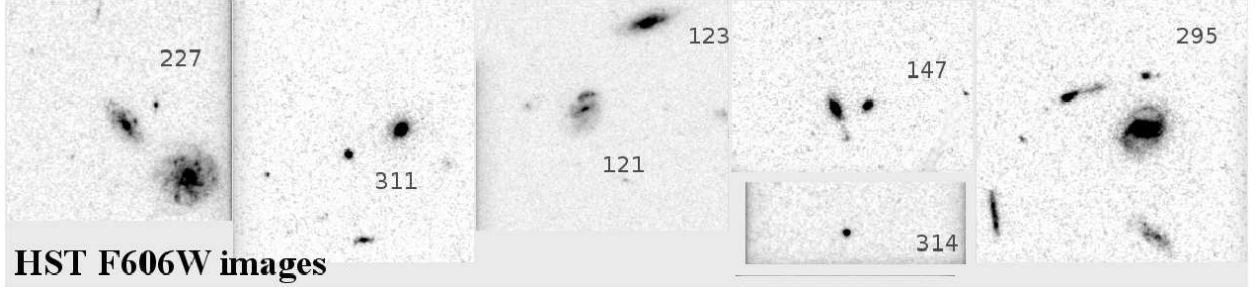


**Figure 3.** Images of seven galaxies extracted from HST ACS *F606W* (HST Legacy Archive, <http://hla.stsci.edu/hlaview.html>) near the GRB 021004 position within the field of size  $3''.5 \times 3''.5$ . The object numbers from the HST ACS catalog are indicated. The table 2 contains the estimates of photometric  $z$ , with the probability of the photo- $z$  measurements for these seven galaxies with known morphology, see the text.

**Table 3.** The absorption Mg II  $\lambda\lambda 2796, 2803\text{\AA}$  doublet identified in [18] in spectra of GRB 021004

GRB	$z_{\text{GRB}}$	$z_{\text{abs}}$	$W_r(\lambda 2796\text{\AA}), \text{\AA}$
		0.5550	$0.248 \pm 0.025$
021004	2.3295	1.3800	$1.637 \pm 0.020$
		1.6026	$1.407 \pm 0.024$

magnitude–error diagram for objects extracted from the GRB 021004 field in BTA ( $R, I$ ) (left) and HST ACS ( $F606W, F814W$ ) (right) optical bands agree satisfactorily. This corresponds to the fact that the transmission curves of the filters mentioned above are the closest to each other in central wavelengths, half-widths and maxima (Fig. 2).

Besides studying host galaxies of GRBs, prompt spectroscopy of their afterglows has revealed (in the optical) such intervening absorption systems as found in the past with quasar spectroscopy. One of such systems is Mg II ( $\lambda\lambda 2796, 2798\text{\AA}$  at rest frame), which is strong and ease to detect in moderate  $S/N$  spectra. Using a large sample of GRB afterglows, an overdensity (the factor 2–4) of strong absorption line systems along the lines of sight has been found [17–19]. We use these data in this work for direct confirmation of the overdensity excess of field galaxies with the peak near  $z \sim 0.56$  around the GRB 021004 position.

Along with photometric and spectral methods in studies of GRB fields, we also include photometry of clusters in new catalogs of galaxy clusters with the purpose to confirm such a peak in  $z$  and to estimate angular size of the whole inhomogeneity in distribution of galaxy clusters, i.e. superclusters at  $z \sim 0.56$ .

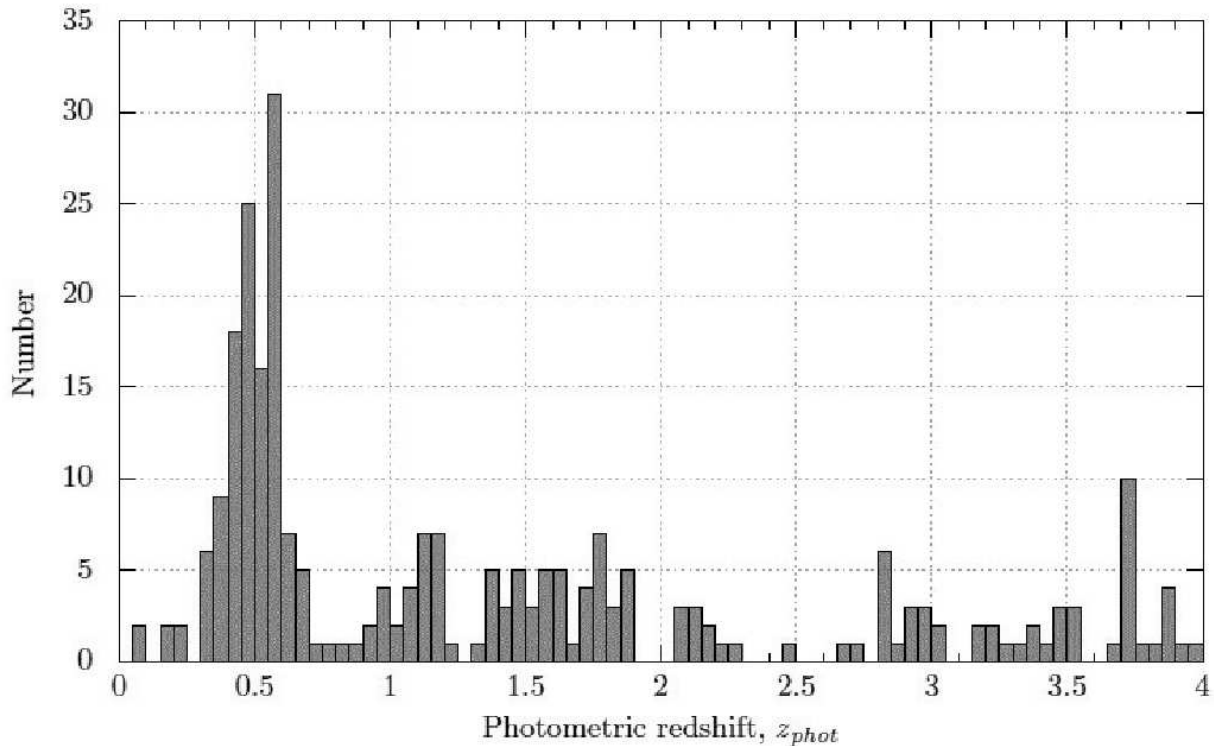


**Figure 4.** The photometric redshift distribution for 246 objects with the peak at  $z \approx 0.56$  based on BTA *BVRI* data.

### 3. THE PHOTOMETRIC REDSHIFT DISTRIBUTION OF GRB 021004 FIELD GALAXIES AND THE MG II $\lambda\lambda 2796, 2803\text{\AA}$ ABSORPTION DOUBLET AT $Z \approx 0.56$ IN THE GRB 021004 AFTERGLOW SPECTRUM

The main idea of the photometric redshift estimations is as follows [23]: the object multicolor photometry may be considered as some very low-resolution spectrum (more specifically, as an energy distribution in several bands), which is used to define redshifts for many (up to several hundreds) objects at once.

In practice, we estimated the photometric redshifts for the extended objects of our BTA sample using the Hyperz software package – a public photometric redshift code [24]. The method is based on finding the best fit of template spectra of various galaxy types, used in the photometric redshift calculation. The template spectra used in our photometric redshift calculation were also taken from [24]. The input data for Hyperz were: the apparent magnitudes of the objects in four *BVRI* bands, the internal extinction law and the redshift range, in which the solution is applied (we considered  $z$  from 0 to 4). We used the extinction law provided by Calzetti et al. [25] for starburst galaxies, which is most commonly used for studies similar to our own as in the above-mentioned



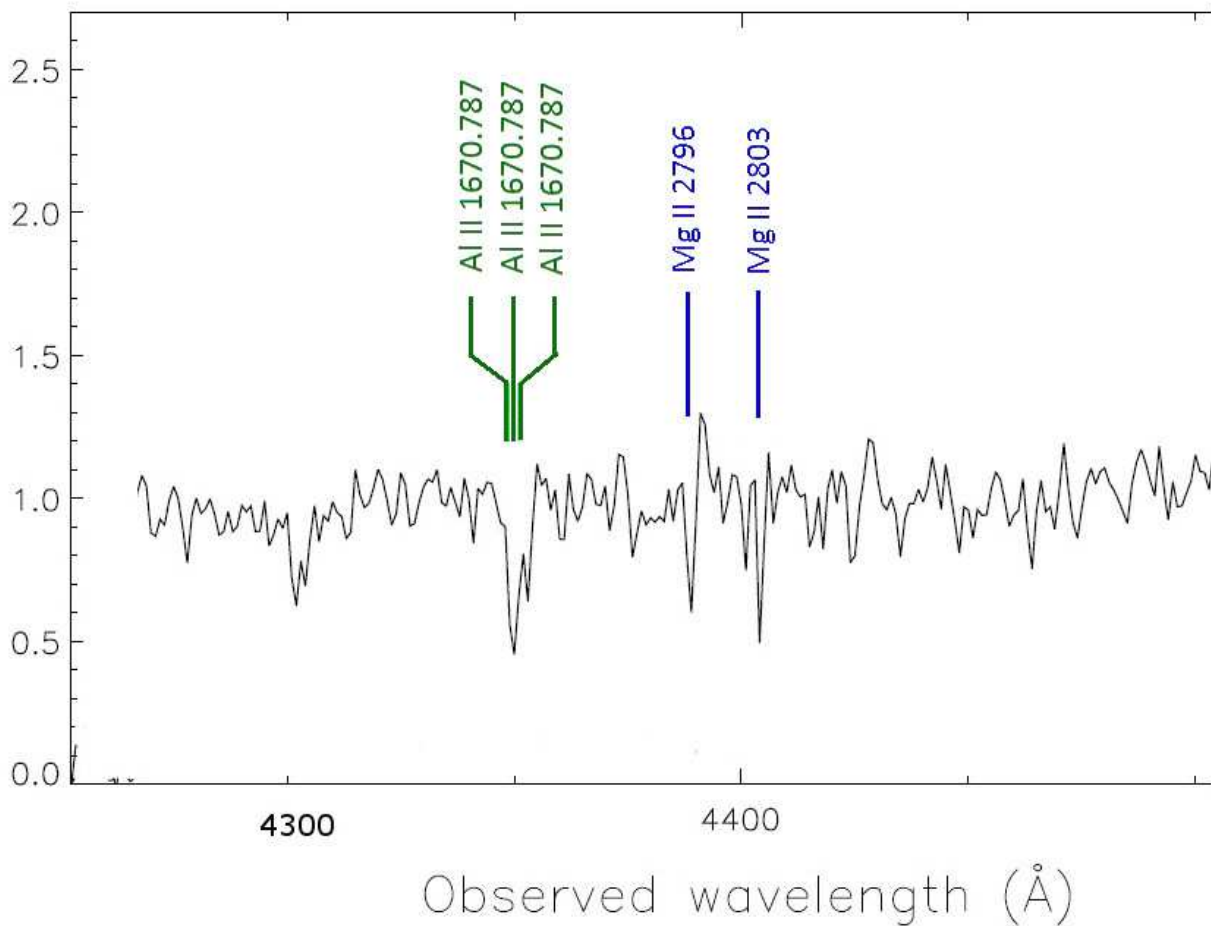


**Figure 5.** Features of VLT/UVES spectra near  $4400\text{\AA}$  with absorption could be interpreted as MgII doublet redshifted at  $z \approx 0.56$ .

work [26], where the application of the Hyperz method is described in more detail and which was applied there for interpretation of observational BTA data.

For seven bright galaxies (with  $R = 20^{\text{m}}6\text{--}21^{\text{m}}8$ ) in the BTA GRB 021004 field we found that models using the spectra from [24] and assigned to these galaxies are in good agreement with HST ACS data. The later are directly revealing the morphology of these objects thanks to the better angular resolution of the HST images (see Fig. 3). Table 2 contains the estimated probability of the photometric redshift  $z \approx 0.4$  thus showing the importance of the initial model spectra or template spectra (or spectral energy distributions—SEDs) of various galaxy types, when the morphology of galaxies from BTA observations can be determined only by their spectral energy distributions for fainter objects, etc. (The standard SEDs for the Hyperz fitting procedures can be taken from <http://webast.ast.obs-mip.fr/hyperz> [24]). So, using BTA observations of the

GRB 021004 field in *BVRI* bands for the spatial (redshift) distribution of field galaxies, we have found a large inhomogeneity with a maximum in the photometric redshift distribution (see Fig. 4) at  $z \approx 0.56$  for 246 objects (from 935 objects, Fig. 1) in the GRB field with the probability of redshift measurements [26] about 90% and more (up to 99%). The difference of these redshifts estimates, for  $z < 1$  at least, from spectral  $z$  is about 10% (see the next section), which is high enough for statistical study of objects properties (more exactly, here we are interested in redshifts of objects with  $0 < z < 0.7$ ; see below).

Certainly, comparison of our data with those of HST (Fig. 1 and Fig. 3) is not yet a significant test of redshift determination near the peak  $z \approx 0.56$  in Fig. 4. That is why below we also use VLT/UVES spectral observations of this GRB afterglow. The GRB 021004 afterglow spectrum has been measured by two teams [18, 19]. The spectrum from [19] shows evidence of Mg II  $\lambda\lambda 2796, 2803 \text{ \AA}$  doublet redshifted at  $z = 1.3820$  and  $z = 1.6020$  (see Fig. 1 in [19]). This spectrum also includes two features that could be identified as Mg II doublet (in the GRB 021004 line of sight) redshifted at  $z \approx 0.5550\text{--}0.5570$ : see Fig. 5 from [19] and results of identification on the earlier spectrum of this burst from [18] in Table 3.

#### 4. ON THE GALAXY CLUSTERING WITH AN EFFECTIVE PEAK NEAR $Z \sim 0.56$ FOR THE PHOTOMETRIC AND SPECTRAL REDSHIFT DISTRIBUTIONS FROM CATALOGS, AND ON THE CMB INHOMOGENEITY IN PLANCK AND GRB 021004 FIELD

The peak near  $z \approx 0.56$  in distribution of redshifts for galaxy clusters near the GRB 021004 position was also tested considering catalog data of both spectral and photometric redshifts. We selected objects in  $3^\circ \times 3^\circ$  area centered to the coordinates RAJ =  $00^{\text{h}}22^{\text{m}}44^{\text{s}}$ , DecJ =  $+17^\circ 40' 58''$  (Fig. 6). The total list of catalogs used for this purpose (with their depths and the number of objects found) is given below:

- redMaPPer DR8 cluster catalog [27, 28]: the catalog depth is  $m_i < 21^{\text{m}}0$  for photometric redshifts, 44 clusters with  $z_{\text{ph}}$ ;
- Group catalogues of the local Universe [29]: the depth of the catalog is  $m_r < 17^{\text{m}}77$  for photometric redshifts, 44 clusters with  $z_{\text{sp}}$ ;
- Rich Clusters of Galaxies [30]: the catalog depth is  $m_B < 23^{\text{m}}$  for spectral redshifts, two clusters with  $z_{\text{sp}}$ ;

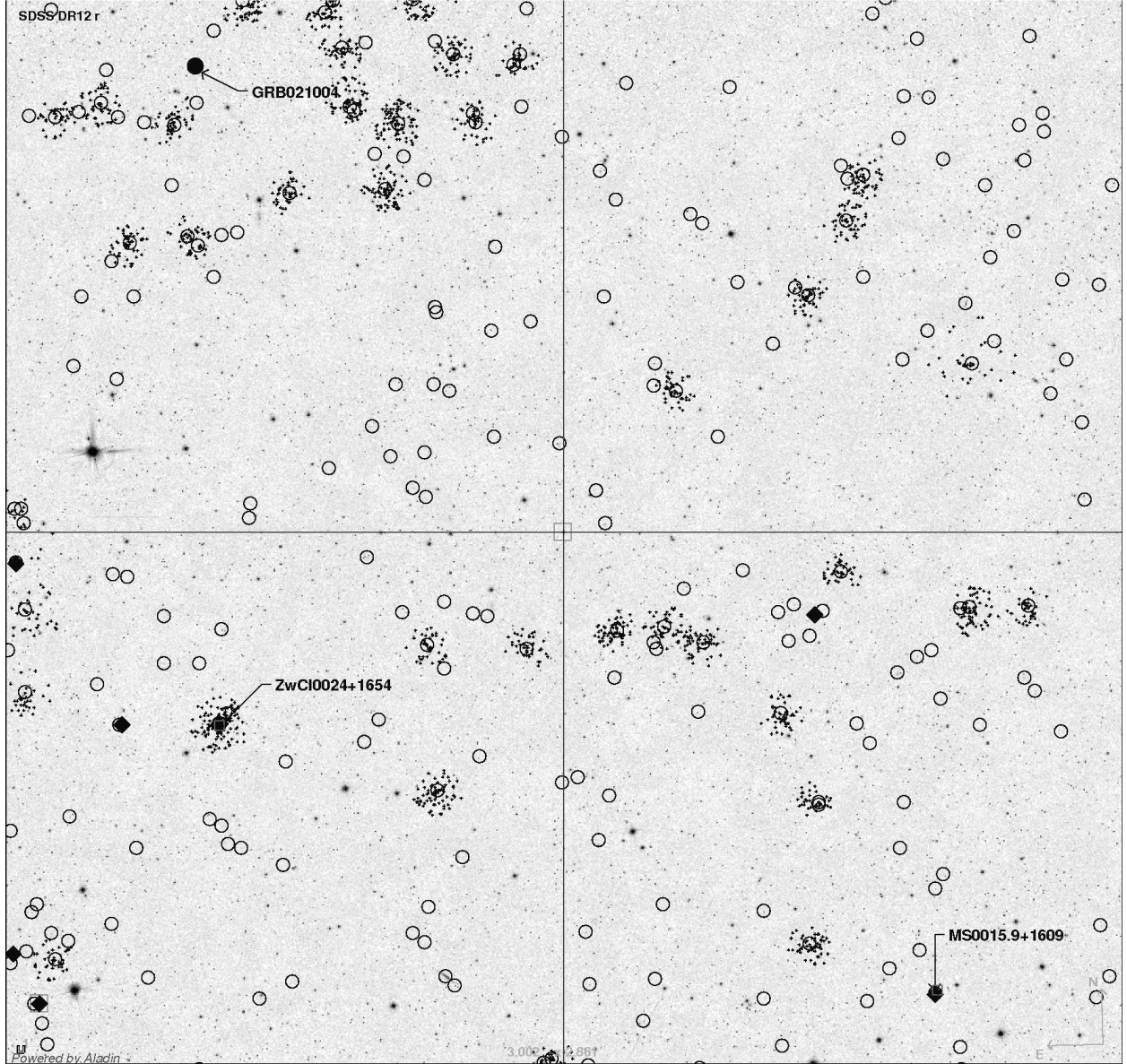


**Figure 6.** Area of  $3^\circ \times 3^\circ$  size encompassing the locations of the gamma-ray burst GRB 021004 (marked with filled circle) and two known rich clusters—CL 0024+1654 ( $z = 0.390$ ) and MS 0015.9+1609 ( $z = 0.541$ ).

Other galaxy clusters from different catalogs (248 in total) are marked. The empty circles correspond to centers of galaxy clusters from the catalogs redMaPPer [24], NOCS [32], WHL [31, 34] and the works by Saulder et al. [29], Oguri [33] and Tempel et al. [35]. The diamonds mark the rich clusters from Abell and Zwicky catalogs [33]. Small clumping crosses mark the galaxies—members of clusters from the catalog

redMaPPer [27, 28].

- Newly rich galaxy clusters identified in SDSS-DR12 [31]: the depth of the catalog is  $m_r < 21^m5$  for photometric redshifts, 128 clusters with  $z_{sp}$  and  $z_{ph}$ ;

- Northern Optical Cluster Survey III [32]: the catalog depth is  $21^m5$ ,  $21^m0$  and  $20^m3$  in  $g$ ,  $r$  and  $i$  for photometric redshifts, 101 clusters with  $z_{\text{ph}}$ ;
- Richness of galaxy clusters [33]: the depth of the catalog is  $m_i < 21^m0$  for photometric redshifts, 74 clusters with  $z_{\text{ph}}$ .

The mosaic halftone image presented in Fig. 6 is obtained thanks to the SDSS SAS<sup>2</sup> from the co-adding of 690 fields in the band  $r$ . The field contains two X-ray neighboring galaxy clusters CL0024+1654 ( $z = 0.390$ ) and MS 0015.9+1609 ( $z = 0.541$ ) at angular distances of about one-two degrees from GRB 021004. Figure 7 shows only the north-east part (upper left square) of the whole region shown in Fig. 6, namely, the region of about  $1^\circ5 \times 1^\circ5$  in size including the GRB 021004 location.

In Fig. 8 the histograms of photometric and spectral redshift distributions for galaxy clusters in this  $1^\circ5 \times 1^\circ5$  size region near GRB 021004 location (Fig. 7) are shown. The redshift distribution of clusters in this region concentrates towards at least three peaks when using these new catalogs: redMaPPer [27], NOCS [32], WHL [31, 34].

Figures 9a–9c show the histograms of differential counts of redshifts for galaxy clusters found in the whole region of about  $3^\circ \times 3^\circ$  size with the center at RAJ =  $5^\circ68$  ( $00^{\text{h}}22^{\text{m}}43^{\text{s}}$ ), DecJ =  $17^\circ68$  ( $17^\circ40'48''$ ) (Fig. 6). All six catalogs (eight tables from VizieR database) were used—see the beginning of the Section.

Thus the photometric redshifts estimated from the deep BTA  $BVRI$  photometry turn out to be quite acceptable, as follows from comparison with data of these catalogs—we see the same peak with  $z \approx 0.56$  in the redshift distribution for galaxy clusters near the GRB 021004 position from catalog data in the region with approximately  $1^\circ5 \times 1^\circ5$  size and even more—in the area with size of about  $3^\circ \times 3^\circ$  at least.

*A practical remark.* A peculiarity detected when building these distributions should be noted. If the catalog data for this field (centered at the position  $5^\circ68; +17^\circ68$ , with the box size of  $3^\circ \times 3^\circ$ ) are selected directly from the VizieR database, then the query result actually somewhat exceeds the given size: the distance between the outermost objects in the right ascension is about  $11192'' = 3^\circ6'32''$ . Thus, in fact, VizieR gives a field of  $3^\circ1 \times 3^\circ0$  size, i.e. more objects are found. This leads to the fact that histograms analogous to those shown in Fig. 9 and built from catalogs will slightly differ due to inclusion of these objects, which should be taken into account with repeating these  $z$  distributions.

---

<sup>2</sup> Science Archive Server, <https://dr12.sdss.org/mosaics>

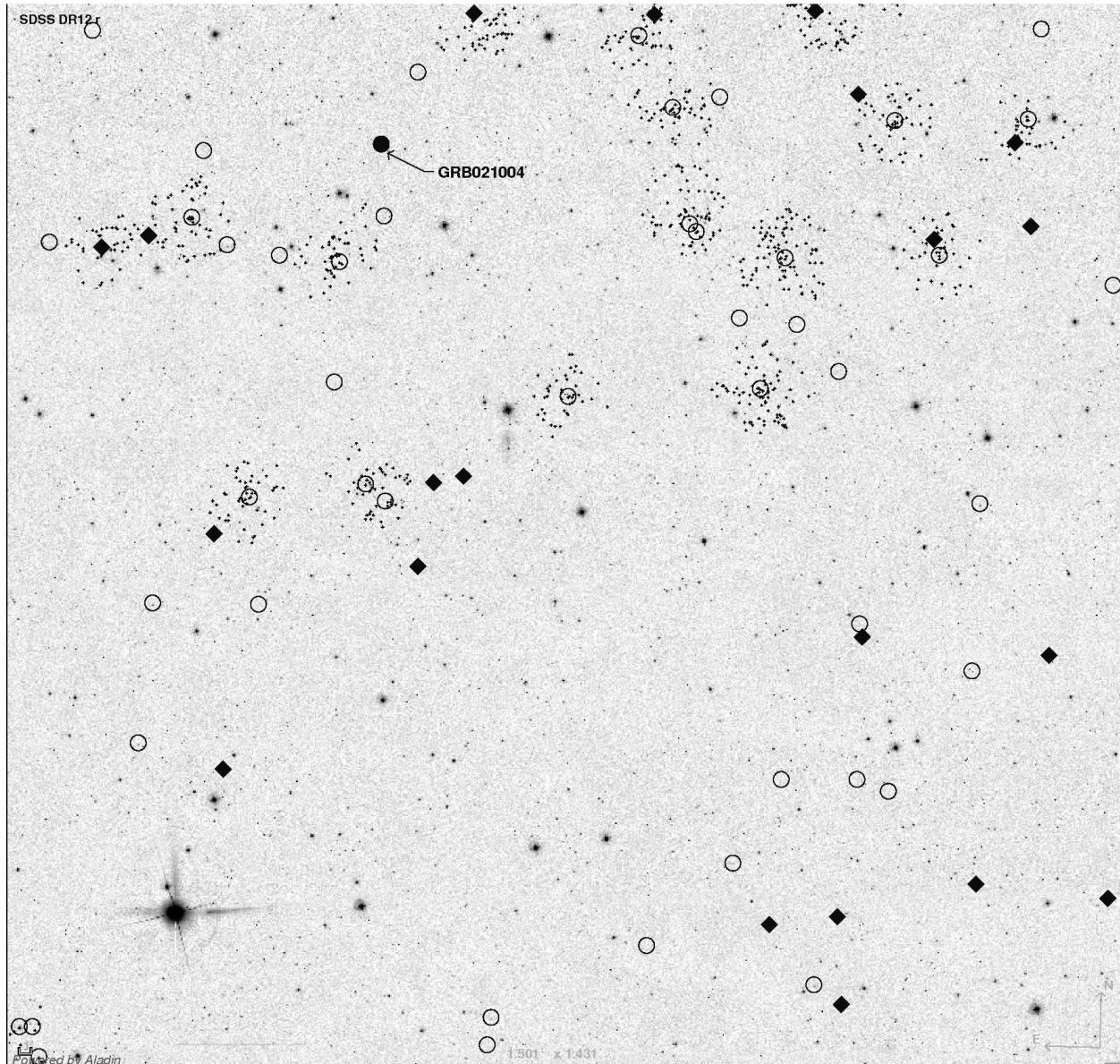


**Figure 7.** The north-east part of the region shown in Fig. 6 (see its upper left square). The area size is about  $1.5 \times 1.5$ . The notations are the same as in Fig. 6.

In Fig. 10 the optical image of Fig. 6 is overlaid on the *Planck* CMB (SMICA) map<sup>3</sup>. The image contains locations of GRB 021004 and two galaxy clusters CL 0024+1654, and MS 0015.9 with X-ray source in them. These two clusters are placed near white areas in Fig. 6 corresponding to minima in the cosmic microwave background (CMB) flux, what may be connected with the Sunyaev–Zeldovich effect observed in such X-ray clusters.

Thus, using SDSS DR12 data, we studied also a larger, of approximately  $3^\circ \times 3^\circ$ , region in-

<sup>3</sup> <http://pla.esac.esa.int/pla>

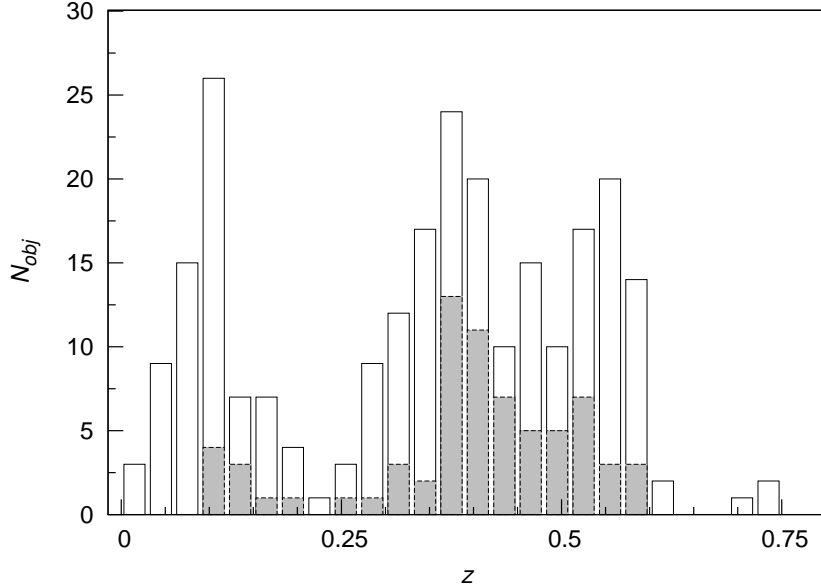


**Figure 8.** The histograms of redshift distributions for clusters in the region near GRB 021004 location (Fig. 7): photometric and spectral redshifts, and only spectral ones –light and grey bins respectively.

cluding these two X-ray clusters. The depth of this survey is about  $22^m$ , and its catalog includes photometrical  $z$  (their distribution is shown in Fig. 9a) and determinations of spectral redshifts for sufficiently bright objects of the survey (the distribution is presented in Fig. 9b). In the whole region (of about  $3^\circ \times 3^\circ$ ), as well as in the region with GRB 021004 location ( $\approx 1.5 \times 1.5$  in size) shown in Fig. 7, the redshift distribution of galaxy clusters also demonstrates an obvious peak at  $z \sim 0.56$  (see Figs. 8 and 9a, 9b, and 9c) for photometrical and spectral redshifts.

As it is seen in Figs. 7 and 9, two X-ray clusters CL 0024+1654 ( $z=0.390$ ) and MS 0015.9+1609 ( $z=0.541$ ) are located very close in  $z$  to two peaks at  $z \sim 0.4$  and  $z \sim 0.56$  in the whole region of about  $3^\circ \times 3^\circ$  size centered at RAJ = 5.68 ( $00^h 22^m 43^s$ ), DecJ = 17.68 ( $17^\circ 40' 48''$ ).

## 5. SIZE ESTIMATION OF INHOMOGENEITY IN DISTRIBUTION OF GALAXY CLUSTERS WITH THE PEAK NEAR $Z \approx 0.56$

To study the spatial behavior of the overdensity excess of field galaxies near  $z \sim 0.56$  around the GRB 021004 position we considered also the redshift distributions in adjacent areas. Relative position of the regions under consideration is shown in the layout of Fig. 11. The central part B2 of about  $3^\circ \times 3^\circ$  size practically coincides with the region shown in Fig. 6. It is surrounded by eight fields of identical size.

Using the same six above-mentioned catalogs [27–33] we selected all galaxy clusters with known

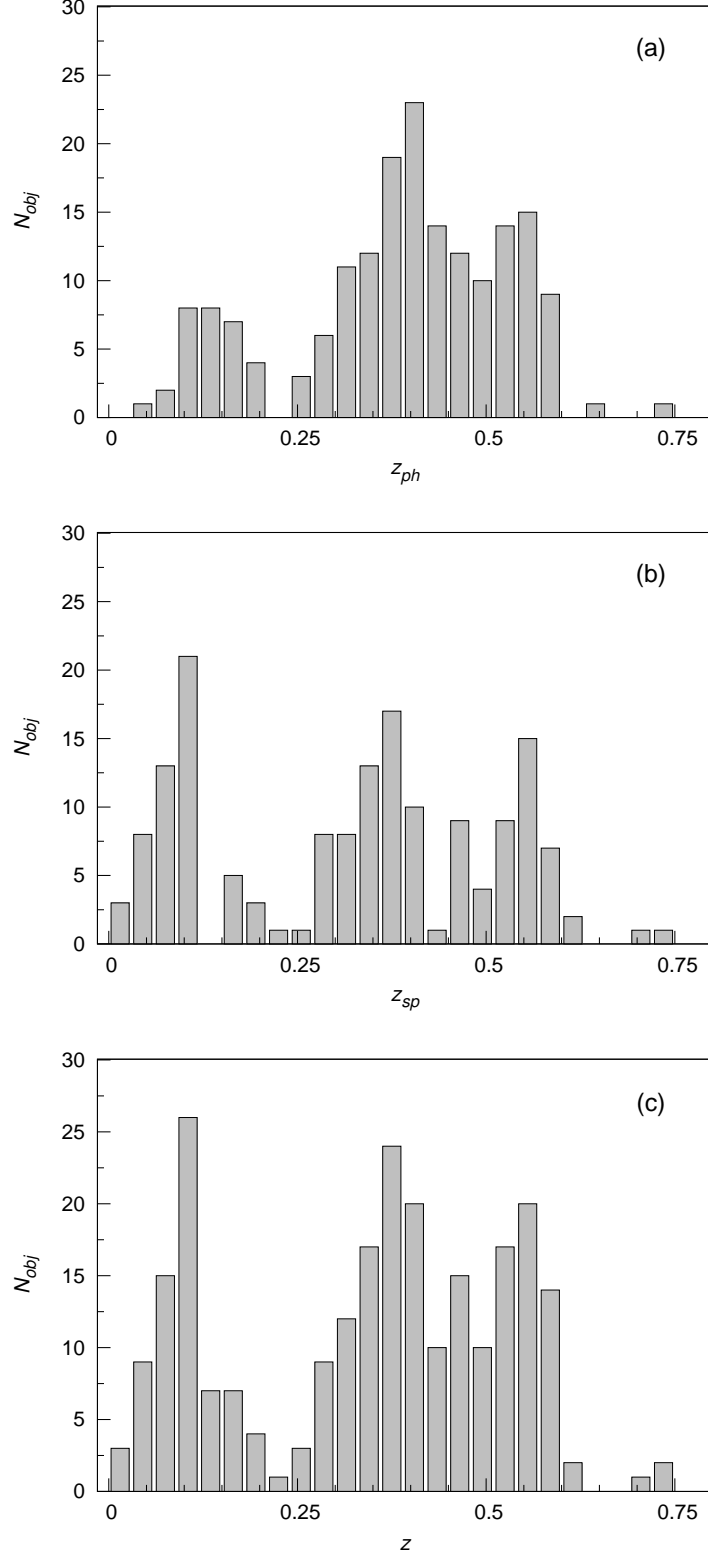


**Figure 9.** Differential counts of redshifts for galaxy clusters from six catalogs mentioned in Section 4 considering a region of about  $3^\circ \times 3^\circ$  size centered at  $RAJ = 5^\circ 68$  ( $00^h 22^m 43^s$ ),  $DecJ = 17^\circ 68$  ( $17^\circ 40' 48''$ ): (a) photometric redshifts (180 clusters), (b) spectral ones (160 clusters) and (c) spectral and photometric redshifts (248 clusters).



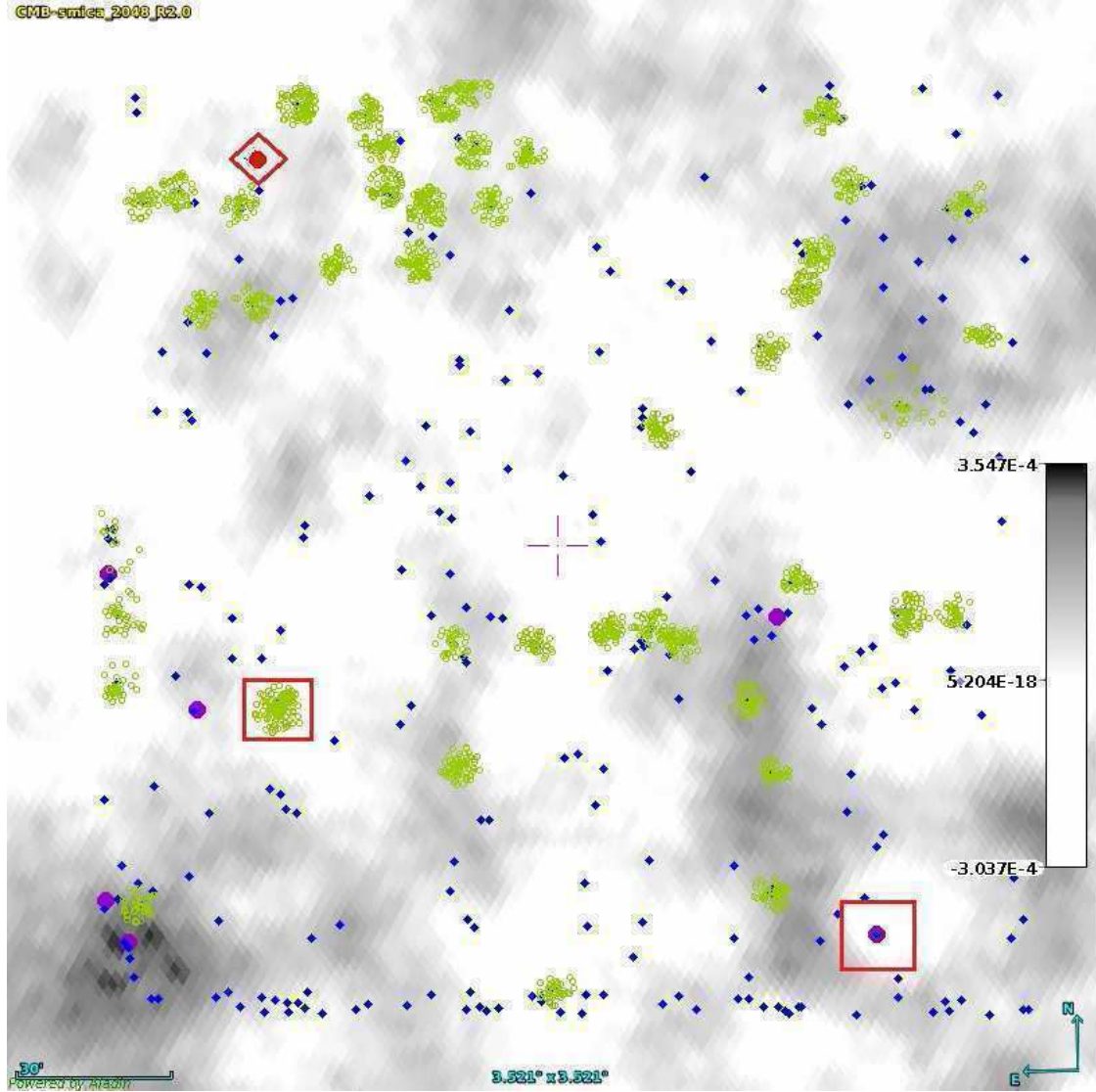


**Figure 10.** The same region as in Fig. 6, but the size is  $3.5^\circ \times 3.5^\circ$ . The image is a CMB map (SMICA) from archives of the *Planck* mission. Two known rich clusters CL 0024+1654 ( $z = 0.390$ ) and MS 0015.9+1609 ( $z = 0.541$ ) and other galaxy clusters from the catalogs are marked. The circle (outlined by a diamond) marks the GRB 021004 location. The full circles show the location of Abell and Zwicky clusters, diamonds show the location of clusters from the catalogs redMaPPer [27], NOCS [32], WHL [31, 34] and the works by Saulder et al. [29], Oguri [33] and Tempel et al. [35].

average (photometric and spectral) redshifts in 8 regions surrounding the central region B2. Applying the method as given in Section 4 for the central region B2 (with the highest peak at about  $z \approx 0.56$ ), we have built  $z$  distributions of galaxy clusters analogous to those shown in Fig. 9 for each of these eight regions.

Figure 12 presents histograms of  $z$ -distributions only for four of nine fields (B1, B2, C1, C2), where the number of detected galaxy clusters near  $z \sim 0.56$  is the largest (the north-west square in



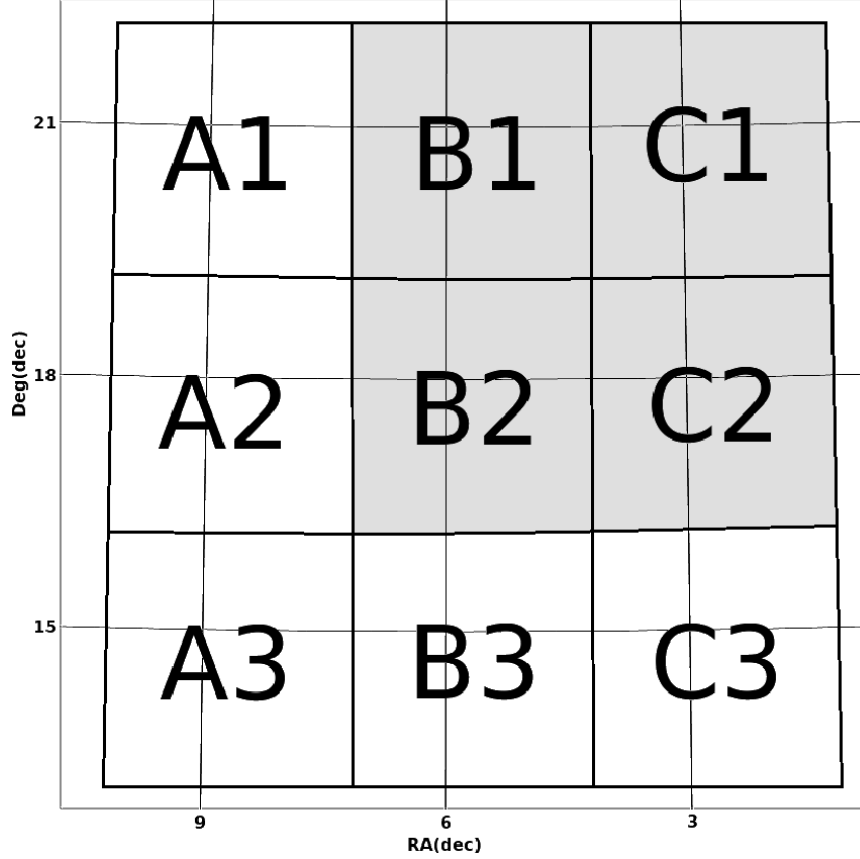


**Figure 11.** The layout of eight regions surrounding the central region B2.

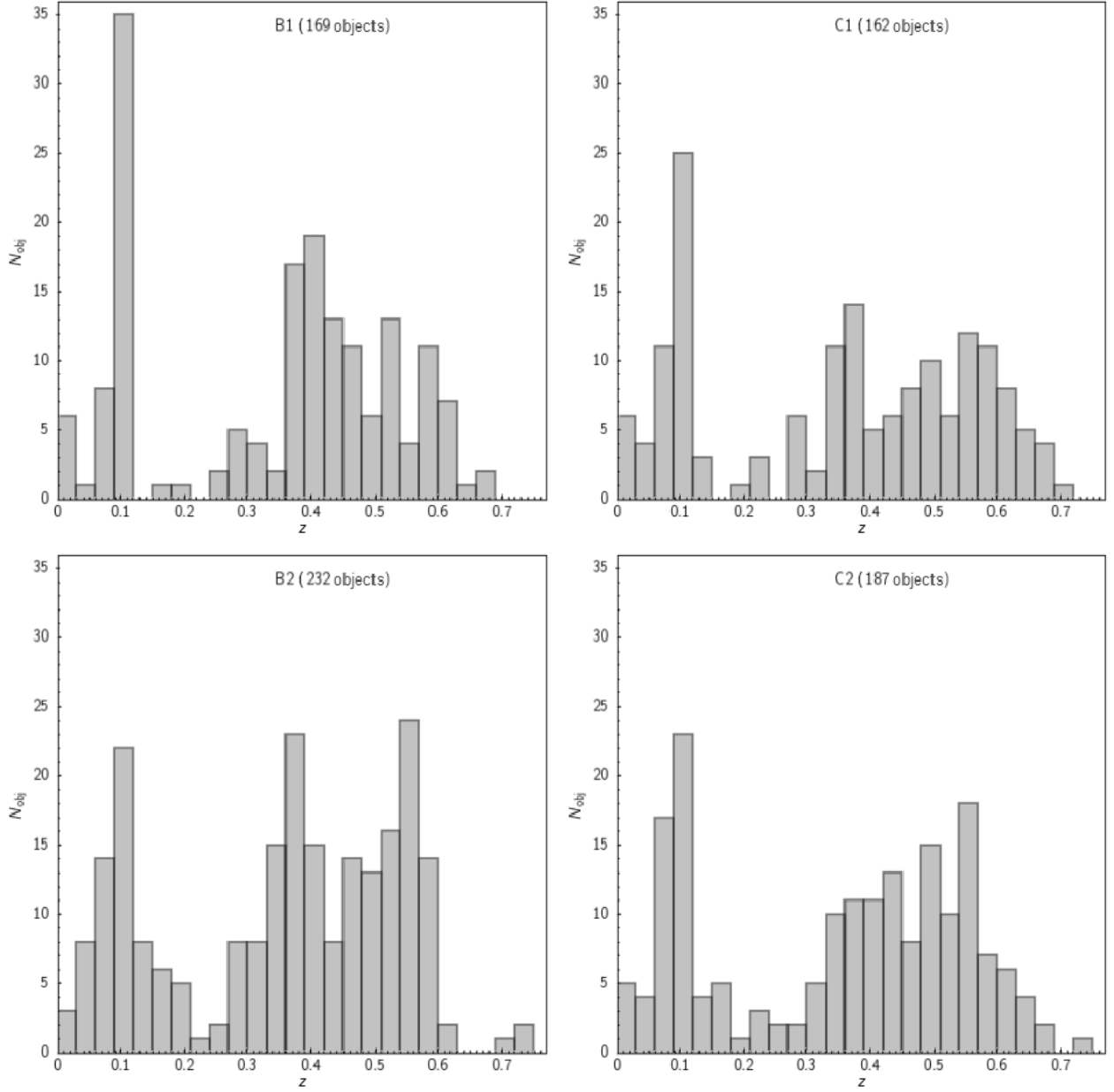
Fig. 11). As is seen, the peak near  $z \sim 0.56$  in these distributions is only seen in the B2, C1 and C2 regions. In the region B1 the number of galaxy clusters with this  $z$  is less.

Figure 13 shows the direct images of four fields B1, B2, C1, C2 corresponding to the layout of Figure 11 and histograms in Fig. 12 (a square of size  $6^\circ \times 6^\circ$ ) where the number of detected galaxy clusters near  $z \sim 0.56$  is the highest. In Fig. 13 the catalog objects—the centers of galaxy clusters—with redshifts near the peak at  $z \approx 0.56$  are marked.

Thus, from catalog data (certainly, with allowance made for their depths) one can estimate the size of the overdensity excess as about  $6^\circ$ – $8^\circ$  in distribution of galaxy clusters with the peak near  $z \approx 0.56$ .

## 6. DISCUSSION AND CONCLUSIONS

The main idea of this work is to reveal the signatures of field galaxies clustering in the GRB021004 line of sight. And we tests for reliability any available signatures of the clustering in the direction and near the GRB position.



**Figure 12.** Histograms of  $z$  distributions for four fields (B1, B2, C1, C2) where the number of detected galaxy clusters near  $z \sim 0.56$  is the highest—the north-west square in the layout of Fig. 11. At the top of each histogram there is the name of the field for which it was built and the number of objects with known  $z$  from catalogs in it.

- The first signature is the BTA GRB 021004 deep field (with a size of about  $4' \times 4'$ ) photometric redshift distribution with a peak near to  $z \sim 0.56$  estimated from BTA multicolor  $BVRI$  photometry in the GRB direction.
- The second signature is the Mg II  $\lambda\lambda 2796, 2803\text{\AA}$  absorption doublet at  $z \approx 0.56$  in the GRB 021004 afterglow VLT/UVES spectra obtained for the afterglow and GRB host galaxy.

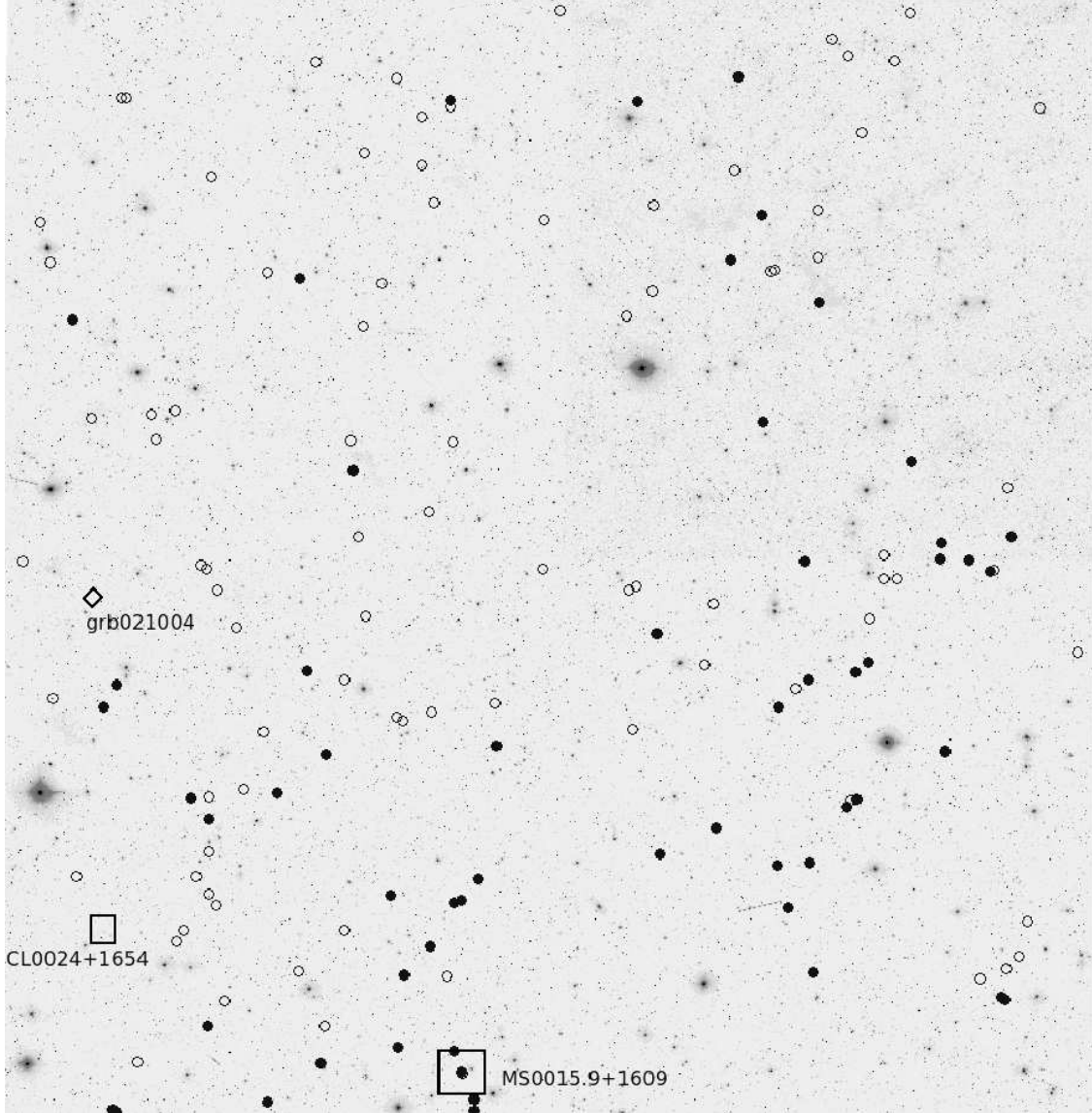


**Figure 13.** Direct images of four fields B1, B2, C1, C2 corresponding to the layout in Fig. 10 and histograms in Fig. 12—a square of size  $6^\circ \times 6^\circ$ . The catalog objects—the centers of galaxy clusters—with redshifts near the peak at  $z \approx 0.56$  are marked. The filled circles denote the objects with redshifts in the range  $0.54 < z < 0.57$  corresponding to the peak bin. The unfilled circles are objects from the adjacent bins  $0.51 < z < 0.54$  and  $0.57 < z < 0.6$ .

- The third signature is the galaxy clustering in a larger ( $\approx 3^\circ \times 3^\circ$ ) area around GRB 021004 with an effective peak near  $z \sim 0.56$  for spectral and photometric redshift distributions from the SDSS and BOSS as a part of SDSS-III.
- And the fourth signature may be some inhomogeneity in the *Planck* field, what may be due to the Sunyaev–Zeldovich effect for galaxy clusters near the GRB 021004 position.
- Also, from data of six catalogs the size of the whole inhomogeneity in distribution of galaxy

clusters with the peak near  $z \approx 0.56$  was estimated to be about  $6^\circ\text{--}8^\circ$ .

In all redshift distributions presented (Figs. 8, 9 and 12) the peak at  $z \approx 0.1$  is obviously distinguished, which corresponds to the well known Sloan Great Wall as a complex of superclusters with a huge size of about  $7^{\text{h}}$  [1, 2]. In the same figures, a peak with  $z \approx 0.4$  is also seen, which can indicate an inhomogeneity in distribution of galaxy clusters near the direction to GRB 021004 with  $z \sim 0.4$ . The same supercluster can also include the X-ray cluster CL0024+1654 with  $z = 0.390$  (see Figs. 6 and 7). The X-ray cluster MS0015.9+1609 with  $z = 0.541$  in Fig. 13, is in the range  $0.54 < z < 0.57$ , corresponding to the peak bin in Fig. 9 with  $z \sim 0.56$ .

The GRB 021004 host galaxy with  $z_{\text{ph}} = 2.225$  is also in Fig. 4 in distribution of photometric redshifts. This  $z_{\text{ph}}$  was measured from BTA *BVRI* photometry for the GRB host galaxy with  $B = 24^{\text{m}}434 \pm 0^{\text{m}}132$ ,  $V = 24^{\text{m}}006 \pm 0^{\text{m}}099$ ,  $R = 24^{\text{m}}174 \pm 0^{\text{m}}154$ ,  $I = 23^{\text{m}}437 \pm 0^{\text{m}}170$ . Correspondingly, the spectroscopic measurements of redshift for GRB 021004 are  $z_{\text{sp}} = 2.3295$  [18] and 2.3304 [19]. Thus, the photometric  $z_{\text{ph}}$  of this galaxy measured by us with BTA corresponds to the spectral  $z$  with the identical error of about 10

Here it should be emphasized that the obtaining of data for estimation of photometric redshift can be done at once for a large sample of galaxies and down to limit depths (see Fig. 1) in the whole GRB field when studying properties of the same host galaxies [16]. At present, the photometric redshifts are already widely used in all modern investigations of galaxy clusters at different  $z$ , which we also use here (see Sections 4 and 5). The new paper [36] deals with application of the photometric redshift method for 1227 galaxies in the Hubble Ultra Deep field down to 30th magnitude (down to  $F775W = 30$ ) in the  $0.4 < z < 1.5$  range. Here we would like also to draw attention to another recent work [37], in which the matter is on photometry in five bands, and the photometric redshift estimations use the galaxy morphology information. This paper shows that by adding galaxy morphological parameters to full  $u, g, r, i, z$ -photometry, only mild improvements are obtained, while the gains are substantial in cases where fewer passbands are available. For instance, the combination of  $g, r, z$ -photometry and morphological parameters almost fully recovers the metrics of five-band photometric redshifts.

When analyzing our BTA *BVRI* data we have considered a redshift range up to  $z = 4$ , though the number of objects with  $z > 1$ , which are bright enough for such analysis, becomes less and less, see Fig. 4. Correspondingly, the uncertainty in estimation of photometric redshifts of such (more and more distant) objects becomes larger according to [26] where the  $z$  estimation errors were studied specially. The limits of catalogs and BTA *BVRI* data are also mentioned at the end of Section 3.

Thus, the results strongly depends on the photometry precision, see Fig. 1. Here we have chosen approximately 10% for the objects under investigation. Correspondingly, for objects at redshifts more than 1 the needed exposure times are larger than those indicated in Table 1. Besides, here the infrared filters can be already needed also. But since here we are interested in the range of intermediate redshifts with  $z < 0.7$ , for which there are already catalog data on photo- $z$  (see at the end of Section 3 + references therein and the beginning of Section 4), we use these photo- $z$  (+ spectro- $z$ ) from catalogs to test our calculations.

Here it should be said also about spectroscopy in the GRB afterglow direction, about our results and (in this connection) about new observational tasks.

A comprehensive study based on a spectroscopic data of 73 GRB afterglows discussing the GRB/quasar overdensity excess of field galaxies around sight-lines was reported [17], included the above-mentioned Mg II  $\lambda\lambda 2796, 2803\text{\AA}$  doublet.

If this excess of intervening systems is real, it should be possible to find an excess of GRB field galaxies around GRB positions, although a preliminary study has revealed no anomalous clustering of galaxies (in comparison with distribution of quasar) at the estimated median redshift of about 0.3 around GRB line of sights [17]. Furthermore, it has been proposed that the majority of short-duration GRBs in early-type galaxies will occur in clusters and three such relationships have been already found [38].

It is also well proven that long-duration GRBs are associated with the core collapse of very massive stars [39–41]. Similarly to core collapse supernovae, the collapse of massive stellar iron cores results in the formation of a compact object (collapsar), accompanied by the high-velocity ejection of a large fraction of a progenitor star mass at relativistic speed producing a series of internal shocks giving rise to the GRB itself [5].

It is known [42] that measurements of the X-ray surface brightness of galaxy clusters (including such as CL 0024+1654 with  $z = 0.390$  and MS 0015.9+1609 with  $z = 0.541$ ) can be used to estimate the angular diameter and distance to these structures. Namely, the determination of distance to supernovae and gamma-ray bursts resulting from collapse of compact objects of stellar mass becomes the main observational task in determining a basic parameter: the total energy release related to such events. The collapse of the massive stellar cores maybe connected with the quark phase transition in the compact objects, which leads to neutrino, gravitational and photon signals from the core collapse supernovae (like SN 1987A) and GRBs. It is also obvious that for low and intermediate redshifts, the sky distribution of electromagnetic and neutrino signals associated with the core collapses can be non-isotropic [43], showing the clustering of galaxies in which the formation of compact objects

occurs due to evolution of massive stars.

In conclusion we would like also to emphasize here that since GRBs are detected at more and more distant cosmological distances with redshifts up to 9.2 [13], this poses additional new questions which are of outmost importance for observational cosmology. What are the redshifts at which the sky distribution of GRBs becomes homogeneous? And what are the redshifts where such bursts (which are related now with collapse of compact objects of stellar mass) are unobservable already?

## ACKNOWLEDGMENTS

The authors are grateful Yu. Baryshev for fruitful discussion and valuable comments.

- 
1. R. K. Sheth and A. Diaferio, *Monthly Notices Royal Astron. Soc.* **417**, 2938 (2011).
  2. M. Einasto, H. Lietzen, M. Gramann, et al., *Astron. and Astrophys.* **595**, A70 (2016).
  3. H. Lietzen, E. Tempel, L. J. Liivamägi, et al., *Astron. and Astrophys.* **588**, L4 (2016).
  4. R. G. Clowes, K. A. Harris, S. Raghunathan, et al., *Monthly Notices Royal Astron. Soc.* **429**, 2910 (2013).
  5. T. Piran, *Phys. Reports* **314**, 575 (1999).
  6. L. G. Balázs, Z. Bagoly, J. E. Hakkila, et al., *Monthly Notices Royal Astron. Soc.* **452**, 2236 (2015).
  7. I. Horváth, J. Hakkila, and Z. Bagoly, *Astron. and Astrophys.* **561**, L12 (2014).
  8. M. L. Khabibullina, O. V. Verkhodanov, and V. V. Sokolov, *Astrophysical Bulletin* **69**, 472 (2014).
  9. C. A. Meegan, G. J. Fishman, R. B. Wilson, et al., *Nature (London)* **355**, 143 (1992).
  10. D. Fargion, arXiv:1408.0227 (2014).
  11. S. Raghunathan, R. G. Clowes, L. E. Campusano, et al., *Monthly Notices Royal Astron. Soc.* **463**, 2640 (2016).
  12. S.-F. S. Chen, R. A. Simcoe, P. Torrey, et al., *Astrophys. J.* **850**, 188 (2017).
  13. V. Sudilovsky, J. Greiner, A. Rau, et al., *Astron. and Astrophys.* **552**, A143 (2013).
  14. M. Arabsalmani, P. Møller, D. A. Perley, et al., *Monthly Notices Royal Astron. Soc.* **473**, 3312 (2018).
  15. T. A. Fatkhullin, A. A. Vasil'ev, and V. P. Reshetnikov, *Astronomy Letters* **30**, 283 (2004).
  16. V. V. Sokolov, T. A. Fatkhullin, A. J. Castro-Tirado, et al., *Astron. and Astrophys.* **372**, 438 (2001).
  17. G. E. Prochter, J. X. Prochaska, and S. M. Burles, *Astrophys. J.* **639**, 766 (2006).
  18. S. D. Vergani, P. Petitjean, C. Ledoux, et al., *Astron. and Astrophys.* **503**, 771 (2009).
  19. A. J. Castro-Tirado, P. Møller, G. García-Segura, et al., *Astron. and Astrophys.* **517**, A61 (2010).
  20. V. L. Afanasiev and A. V. Moiseev, *Astronomy Letters* **31**, 194 (2005).
  21. Y. N. Parijskij, O. P. Zhelenkova, P. Thomasson, et al., *EAS Publ. Ser.* **61**, 439 (2013).
  22. E. Bertin and S. Arnouts, *Astron. and Astrophys. Suppl.* **117**, 393 (1996).

23. W. A. Baum, IAU Symp. **15**, 390 (1962).
24. M. Bolzonella, J.-M. Miralles, and R. Pelló, *Astron. and Astrophys.* **363**, 476 (2000).
25. D. Calzetti, L. Armus, R. C. Bohlin, et al., *Astrophys. J.* **533**, 682 (2000).
26. Y. V. Baryshev, I. V. Sokolov, A. S. Moskvitin, et al., *Astrophysical Bulletin* **65**, 311 (2010).
27. E. S. Rykoff, E. Rozo, D. Hollowood, et al., *Astrophys. J. Suppl.* **224**, 1 (2016).
28. E. S. Rykoff, E. Rozo, M. T. Busha, et al., *Astrophys. J.* **785**, 104 (2014).
29. C. Saulder, E. van Kampen, I. V. Chilingarian, et al., *Astron. and Astrophys.* **596**, A14 (2016).
30. G. O. Abell, H. G. Corwin, Jr., and R. P. Olowin, *Astrophys. J. Suppl.* **70**, 1 (1989).
31. Z. L. Wen and J. L. Han, *Astrophys. J.* **807**, 178 (2015).
32. R. R. Gal, P. A. A. Lopes, R. R. de Carvalho, et al., *Astron. J.* **137**, 2981 (2009).
33. M. Oguri, *Monthly Notices Royal Astron. Soc.* **444**, 147 (2014).
34. Z. L. Wen, J. L. Han, and F. S. Liu, *Astrophys. J. Suppl.* **199**, 34 (2012).
35. E. Tempel, A. Tamm, M. Gramann, et al., *Astron. and Astrophys.* **566**, A1 (2014).
36. J. Brinchmann, H. Inami, R. Bacon, et al., *Astron. and Astrophys.* **608**, A3 (2017).
37. J. Y. H. Soo, B. Moraes, B. Joachimi, et al., *Monthly Notices Royal Astron. Soc.* **475**, 3613 (2018).
38. M.-S. Shin and E. Berger, *Astrophys. J.* **660**, 1146 (2007).
39. H. Yüksel and M. D. Kistler, *Phys. Let. B* **751**, 413 (2015).
40. M.-H. Li and H.-N. Lin, *Astron. and Astrophys.* **582**, A111 (2015).
41. T. N. Ukwatta and P. R. Woźniak, *Monthly Notices Royal Astron. Soc.* **455**, 703 (2016).
42. R. F. L. Holanda, V. C. Busti, L. R. Colaço, et al., *J. Cosmology Astroparticle Phys.* **8**, 055 (2016).
43. A. Gomboc, *Contemporary Physics* **53**, 339 (2012).